Electronic Supporting Information

Metal cation substitution can tune CO_2, H_2O and CH_4 switching pressure in transiently porous coordination networks

Varvara I. Nikolayenko,[a†] Dominic C. Castell,[a†] Debobroto Sensharma,[a] Mohana Shivanna,[b] Leigh Loots,[c] Ken-ichi Otake,[b] Susumu Kitagawa,[b] Leonard J. Barbour[c] and Michael J. Zaworotko[a*]

[a] Department of Chemical Sciences, Bernal Institute, University of Limerick, Limerick V94T9PX, Republic of Ireland.
[b] Institute for Integrated Cell-Material Sciences (iCeMS), Institute for Advanced Study, Kyoto University (KUIAS), Yoshida Ushinomiyacho, Sakyoku, Kyoto 606-8501, Japan.
[c] Department of Chemistry and Polymer Science University of Stellenbosch Matieland 7600, South Africa.

CCDC 2179843-2179848

†These authors contributed equally.
* xtal@ul.ie

List of Contents

1. Ligand Synthesis

General information

Commercially available starting materials and solvents were purchased from Sigma Aldrich, Merck and Fluorochem. All reactions were monitored using aluminium backed silica gel Merck 60 F_{254} TLC plates and visualised using UV irradiation. Column chromatography was carried out with Merck silica gel 230-400 mesh silica gel.

Synthesis of dpt was carried out in two steps, according to a previously reported procedure.[1]

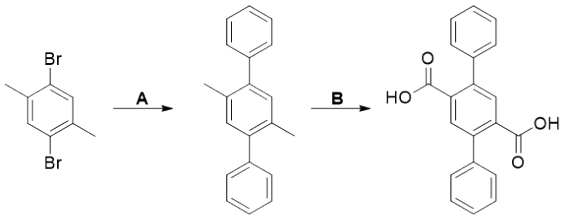

dpt

Scheme S1: Two step synthesis of dpt ligand.

Step A: 20 ml of deionized water was degassed for 30 min using N_2. 2,5-dibromo-*p*-xylene (2.00 g, 7.58 mmol, 1.0 eq), phenyl boronic acid (2.03 g, 16.7 mmol, 2.2 eq), $Pd(OAc)_2$ (3.40 mg, 0.2 mol%), K_2CO_3 (5.24 g, 37.9 mmol, 5.0 eq) and *n*-Bu_4NBr (4.87 g, 15.2 mmol, 2.0 eq) were all added. The resulting suspension was heated to 70 °C for 4 hours and stirred vigorously under an inert atmosphere. After cooling to room temperature, the reaction mixture was diluted further with water (~ 150 ml) and extracted with Pet. ether. The organic phase was dried over $MgSO_4$ and concentrated under reduced pressure to yield 2',5'-dimethyl-[1,1':4'1"]terphenyl as a white solid (1.88 g, 96%).

Step B: 2',5'-dimethyl-[1,1':4'1"]terphenyl (700 mg, 2.71 mmol, 1.0 equiv) was added to 20 ml of pyridine. 2.2 g of $KMnO_4$ in 2.0 ml of H_2O was then added and the reaction mixture was heated to reflux for 2 hours. After reaching reflux, every 30 min, an additional 1.0 g of $KMnO_4$ in 2.0 ml was added (a total of 4 times). After 6 hours at reflux, a final 10 ml of water was added to the reaction mixture, which was then allowed to reflux overnight. The MnO_2 precipitate was then hot filtered from the reaction mixture and washed with boiling water (100 ml). The filtrate was acidified (pH 3-4) using conc. HCl, precipitating the product dpt (732 mg, 85%) as a white solid, which was collected by filtration, washed with 0.2 M HCl and finally dried in a 105 °C oven.

2. Crystallisation

Crystals of **X-dmp-1-M** were grown solvothermally by combining 0.3 mmol (63.0 mg) dpt, 0.3 mmol (95.0 mg) 1,3-bib and 0.3 mmol metal salt (cobalt nitrate hexahydrate (87.0 mg), zinc nitrate hexahydrate (89.0 mg) or cadmium nitrate tetrahydrate (92.0 mg)) in 10 ml DMF and heating at 120 °C. Purple, colourless and pale-yellow block crystals were obtained of each of the respective crystallisations after two days.

3. Single-Crystal X-ray Diffraction

X-ray intensity data were recorded on a Bruker SMART APEX II[2] and a Bruker Quest APEX III equipped with a Mo or Cu sealed tube source. Both diffractometers employ an Oxford Cryosystems 700+ Plus cryostat to control the temperature of the sample. Data reduction was carried out by means of standard procedures using the Bruker software package SAINT.[3] Absorption corrections and correction of other systematic errors were carried out using SADABS.[4] All structures were solved by direct methods using SHELXS-16 and refined using SHELXL-16.[5] X-Seed[6] was used as the graphical interface for the SHELX program suite. Solvent-accessible voids can be visualised by calculating Connolly surfaces using MS-ROLL,[7] another program incorporated into X-Seed. Hydrogen atoms were placed in calculated positions using riding models.

Activation Procedure

A suitable crystal of each as-synthesised phase of **X-dmp-1-M** was selected and glued onto a glass fibre with cyanoacrylate glue. The glass fibre was then inserted into an environmental gas cell (EGC), which consists of a 0.3 mm Lindemann capillary secured to a steel nut with epoxy that is screwed into a valve body. The EGC allows for evacuation/pressurisation of the immediate crystal environment and transportation to a diffractometer. The EGC was then connected to a Pfeiffer Hi-Cube vacuum pump (pressure: ~ 3×10^{-3} mbar) and immersed in oil, which was heated to 393 K overnight. The valve was then closed and the EGC removed from the activation apparatus.

Gas loading of **X-dmp-1-Cd**

The activated crystal of **X-dmp-1-Cd-β** in the EGC was attached to a CO_2 cylinder via a gas manifold (regulator). In an attempt to obtain a single crystal structure of the **X-dmp-1-Cd-γ3** phase, the system was pressurised to the cylinder maximum (56 bar) and left to equilibrate under static pressure for 12 h (multiple equilibration times were tested and this was found to be the best) after which the EGC was closed and loaded onto the diffractometer.

X-dmp-1-Cd-γ1 (56 bar at 298K) CO_2 loaded structure determination

At 56 bar and 298K, the crystal of **X-dmp-1-Cd-β** has converted to **X-dmp-1-Cd-γ1**. The structure was SQUEEZED and the checkcif had the following alert:

Alert level A

```
PLAT201_ALERT_2_A Isotropic non-H Atoms in Main Residue(s) ....... 12 Report
O1 O2 C13 C14 C15 etc.
```

Response: One of the dpt linkers is disordered over two positions with site occupancies of 0.58:0.42. Despite the two very clear positions, additional residual electron density is observed but could not be modelled. As the linker is moving both components of disorder have been intentionally left isotropic.

X-dmp-1-Cd-γ3 (56 bar at 273K) CO_2 loaded structure determination

The same **X-dmp-1-Cd-γ1** crystal was then cooled down to 273 K using the single-crystal X-ray diffraction instrument cryostream and left to equilibrate for several hours at this temperature. The structure was SQUEEZED and the checkcif had the following alert:

Alert level B

```
PLAT234_ALERT_4_B Large Hirshfeld Difference C18 --C19 . 0.27 Ang.
```

Response: This alert is associated with thermal motion present in the dpt linker. Unlike in **X-dmp-1-Cd-γ1**, no second position of disorder could be reliably modelled.

Table S1. Selected crystallographic data for the as-synthesized (α) and activated (β) structures **X-dmp-1-M**.

2111570-2111569 (previously reported) and 2179843-2179848

	X-dmp-1-Co-α	**X-dmp-1-Co-β**	**X-dmp-1-Zn-α**	**X-dmp-1-Zn-β**	**X-dmp-1-Cd-α**	**X-dmp-1-Cd-β**	**X-dmp-1-Cd-γ1**	**X-dmp-1-Cd-γ3**
Ref Code	2111570	2111569	2179847	2179848	2179843	2179844	2179846	2179845
Empirical Formula	$C_{36.14}H_{31.66}CoN_{5.38}O_{5.38}$	$C_{32}H_{21.45}CoN_4O_4$	$C_{38}H_{36}ZnN_6O_6$	$C_{32}H_{22}ZnN_4O_4$	$C_{38}H_{36}CdN_6O_6$	$C_{32}H_{22}CdN_4O_4$	$C_{32}H_{22}CdN_4O_4$ [+ solvent]	$C_{32}H_{22}CdN_4O_4$ [+ solvent]
Formula weight	686.34	584.91	738.10	591.93	785.13	638.95		638.95
Guest	DMF	-	DMF	-	DMF	-	CO_2	CO_2
Temperature (K)	100(2)	298(2)	100(2)	298(2)	100(2)	298(2)	298(2)	273(2)
Wavelength (Å)	0.71073	0.71073	0.71073	0.71073	0.71073	0.71073	0.71073	0.71073
Crystal system	Monoclinic	Monoclinic	Monoclinic	Monoclinic	Monoclinic	Monoclinic	Monoclinic	Monoclinic
Space group	$P2_1/n$	$P2_1/n$	$P2_1/n$	$P2_1/n$	$P2_1/n$	$P2_1/n$	$P2_1/n$	$P2_1/n$
a/Å	10.031(2)	9.843(7)	10.037(8)	9.840(4)	9.610(2)	9.750(1)	9.8420(9)	9.975(2)
b/ Å	14.620(3)	13.890(1)	14.789(7)	13.631(9)	14.733(1)	15.205(5)	15.4247(14)	15.880(4)
c/ Å	23.674(5)	22.608(3)	23.525(5)	21.523(6)	24.975(1)	19.918(2)	23.677(2)	23.467(6)
α°	90	90	90	90	90	90	90	90
β°	99.877(3)	96.289(1)	99.162(1)	92.129(2)	98.561(1)	96.170(3)	97.756(3)	98.276(8)
γ°	90	90	90	90	90	90	90	90
Volume ($Å^3$)	3420.5(1)	3072.6(3)	3447.9(5)	2885.2(2)	3496.7(7)	2935.8(6)	3561.5(5)	3678.5(15)
Z	4	4	4	4	4	4	4	4
Rint	6.52%	7.78%	6.92%	8.17%	5.06%	6.55%	8.61%	10.53%

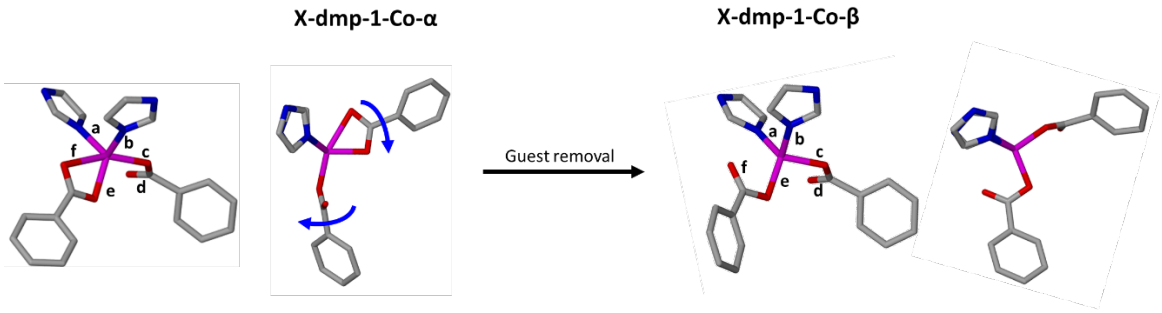

	X-dmp-1-Co-α	X-dmp-1-Co-β	Bond difference (Å)
a	2.02(7) Å	2.01(6) Å	0.01
b	2.03(1) Å	2.03(6) Å	0
c	1.97(2) Å	1.94(9) Å	0.03
d	3.08(7) Å	2.84(2) Å	0.24
e	2.00(9) Å	1.96(7) Å	0.04
f	2.36(8) Å	2.51(8) Å	0.15

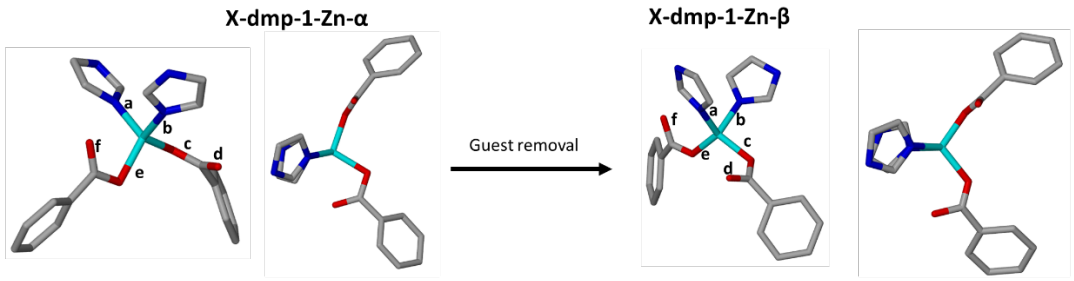

	X-dmp-1-Co-α	X-dmp-1-Co-β	Bond difference (Å)
a	2.02(8) Å	1.99(1) Å	0.03
b	2.00(9) Å	2.05(7) Å	0.05
c	1.95(9) Å	1.92(4) Å	0.03
d	3.09(4) Å	2.80(7) Å	0.29
e	1.98(5) Å	1.91(2) Å	0.07
f	2.58(7) Å	2.91(6) Å	0.33

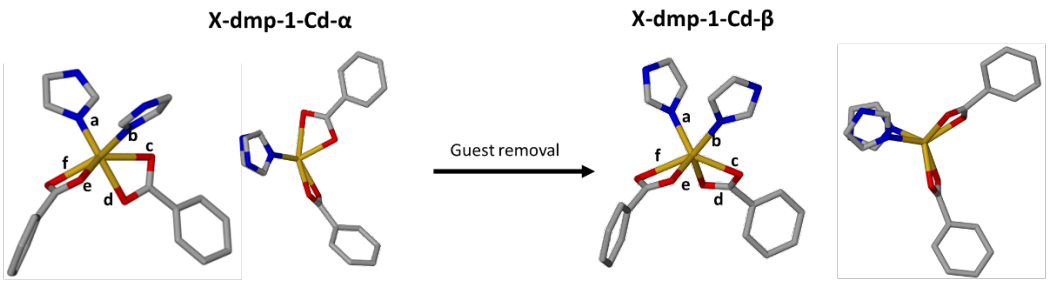

	X-dmp-1-Co-α	X-dmp-1-Co-β	Bond difference (Å)
a	2.22(2) Å	2.26(1) Å	0.04
b	2.27(4) Å	2.32(3) Å	0.05
c	2.51(2) Å	2.28(1) Å	0.23
d	2.23(8) Å	2.35(2) Å	0.12
e	2.29(9) Å	2.19(4) Å	0.10
f	2.43(1) Å	2.60(1) Å	0.17

Fig. S1. Comparison of bonds associated with the metal node in **X-dmp-1-M-α** vs **X-dmp-1-M-β**.

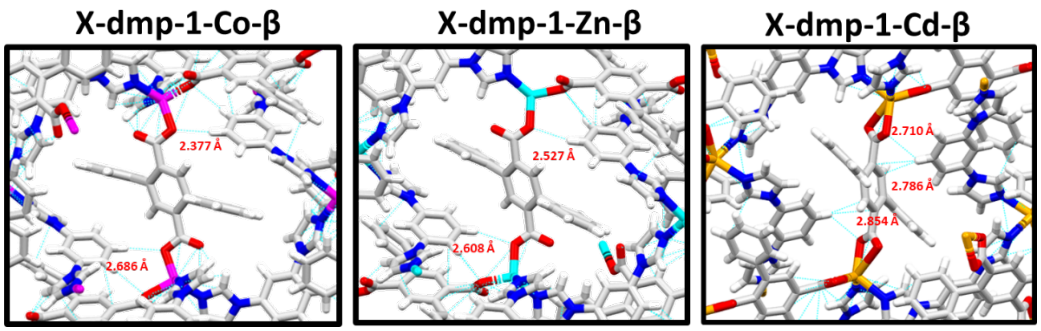

Fig. S2. Comparison of short contacts in all three metal variants of **X-dmp-1-M-β**.

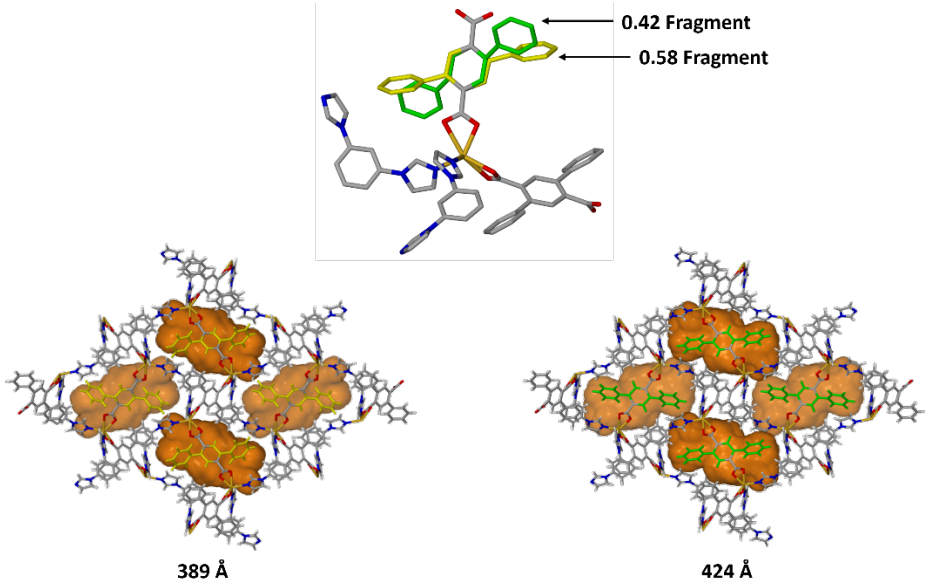

Fig. S3. Packing diagrams of **X-dmp-1-Cd-γ1** showing the two fragments of disorder. Yellow fragment has discrete cavities of 389 $Å^3$ while the green fragment produces cavities pf 424 $Å^3$.

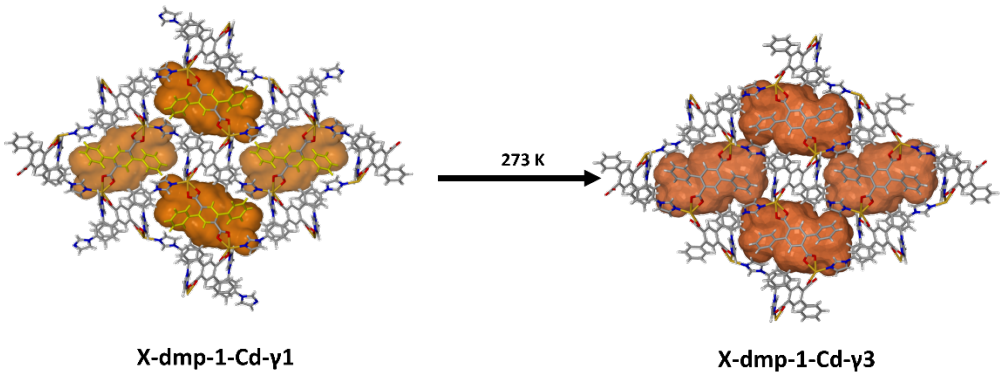

Fig. S4. Packing diagrams of **X-dmp-1-Cd-γ1** (major fragment) and **X-dmp-1-Cd-γ3** showing how the discrete cavities expand to form channels connected by narrow apertures.

4. Powder Xray Diffraction

Powder X-ray diffraction experiments were conducted using microcrystalline samples on a PANalytical Empyrean diffractometer (40 kV, 40 mA, Cu $K_{\alpha 1,2,}$ λ = 1.5418 Å) in Bragg-Brentano geometry. A scan speed of 0.044509 °/s (2.6 °/min), with a step size of 0.0262 ° in 2θ was used at room temperature with a range of 5 °< 2θ < 40 °. Powder samples were evenly distributed on a zero-background holder after being ground with a mortar and pestle to minimise the effects of preferred orientation. Data analysis was carried out using X'Pert HighScore Plus[8] (Version 2.2e). Powder patterns were simulated from SCXRD structures using Mercury.[9]

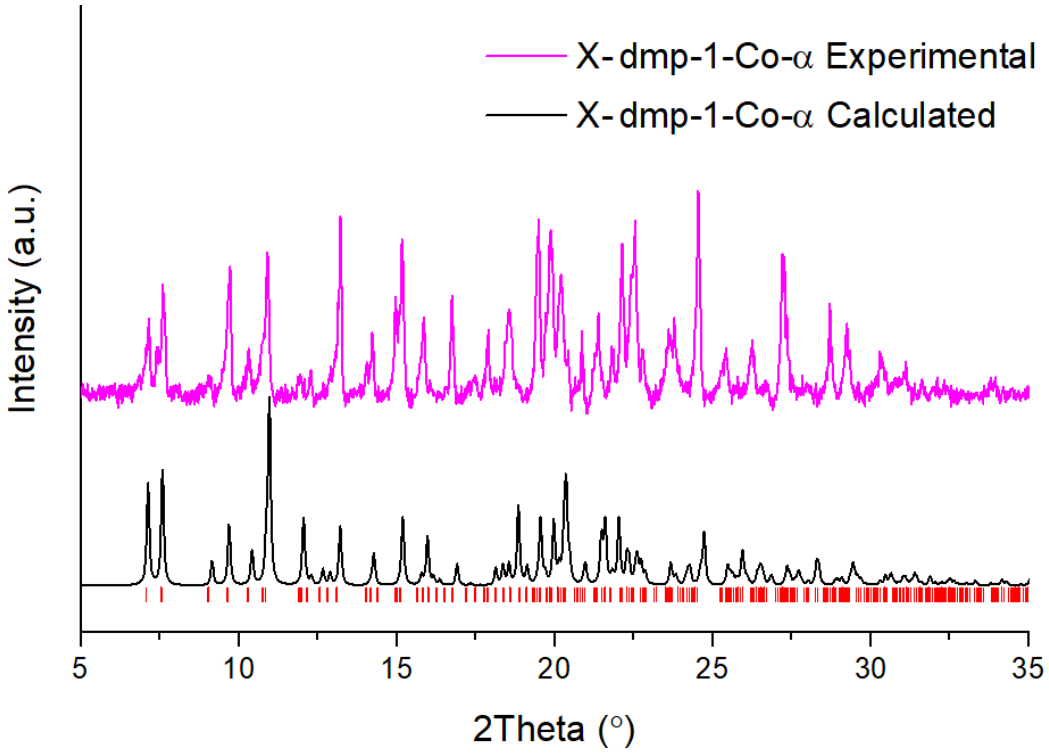

Fig. S5. PXRD patterns of **X-dmp-1-Co- α** calculated from the crystal structure (black), and the experimental pattern (pink) of **X-dmp-1-Co-α**, showing that the SCXRD structure is representative of the bulk material.

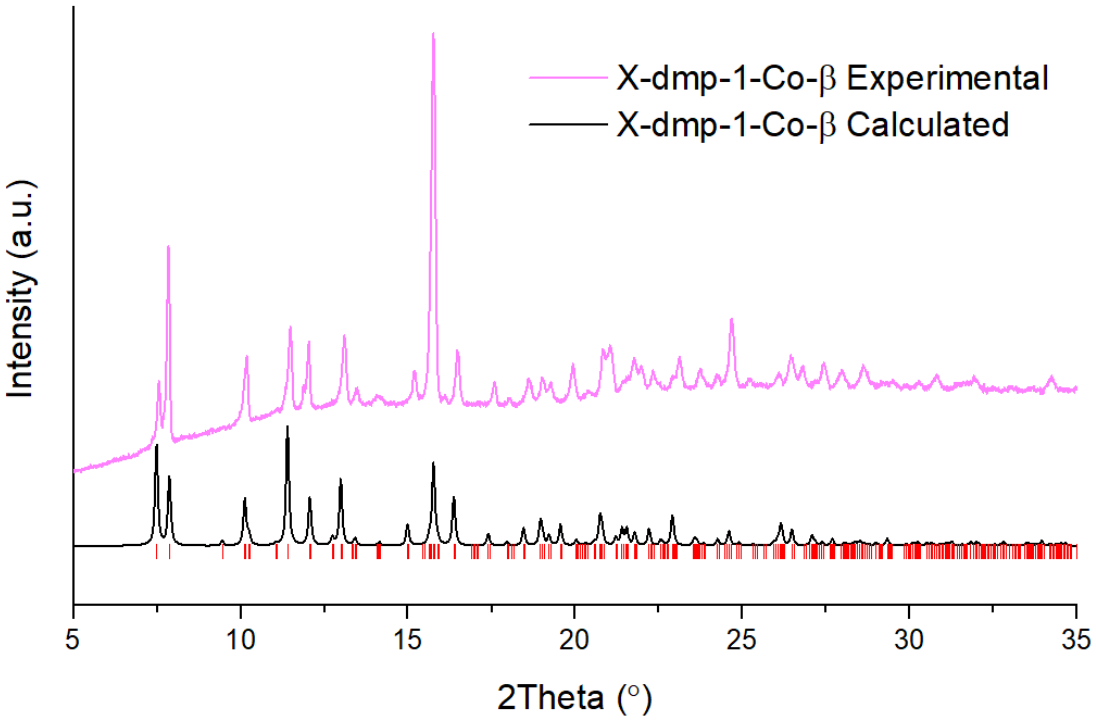

Fig. S6. PXRD patterns of **X-dmp-1-Co-β** calculated from the crystal structure (black), and the experimental pattern (light pink) of **X-dmp-1-Co-β**, showing that the SCXRD structure is representative of the bulk material.

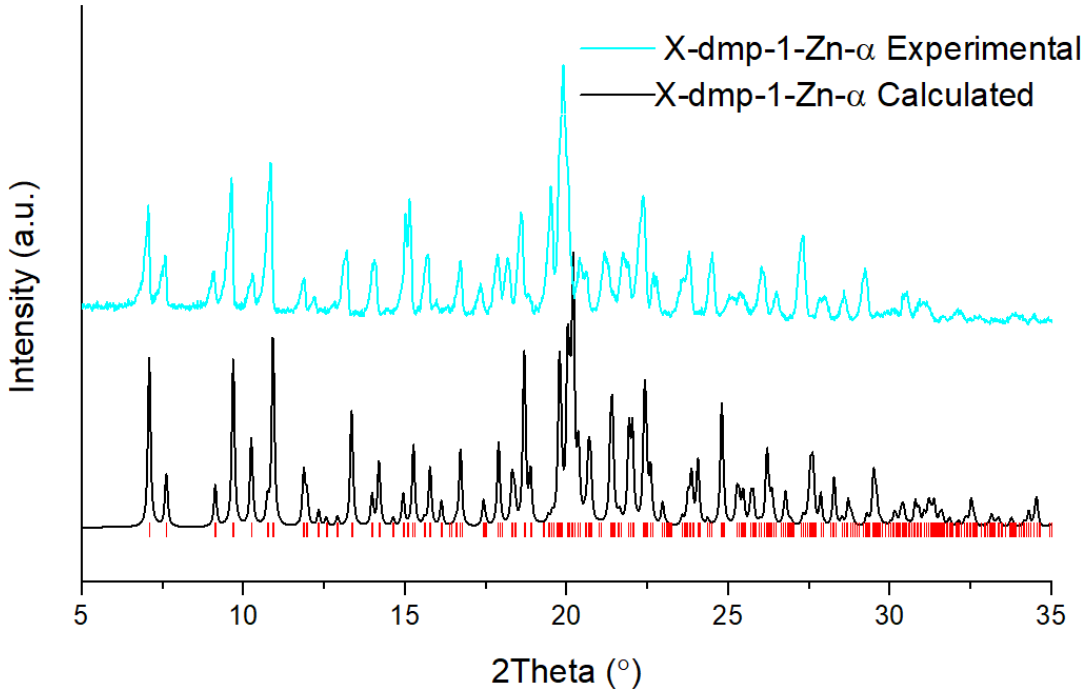

Fig. S7. PXRD patterns of **X-dmp-1-Zn- α** calculated from the crystal structure (black), and the experimental pattern (cyan) of **X-dmp-1-Zn-α**, showing that the SCXRD structure is representative of the bulk material.

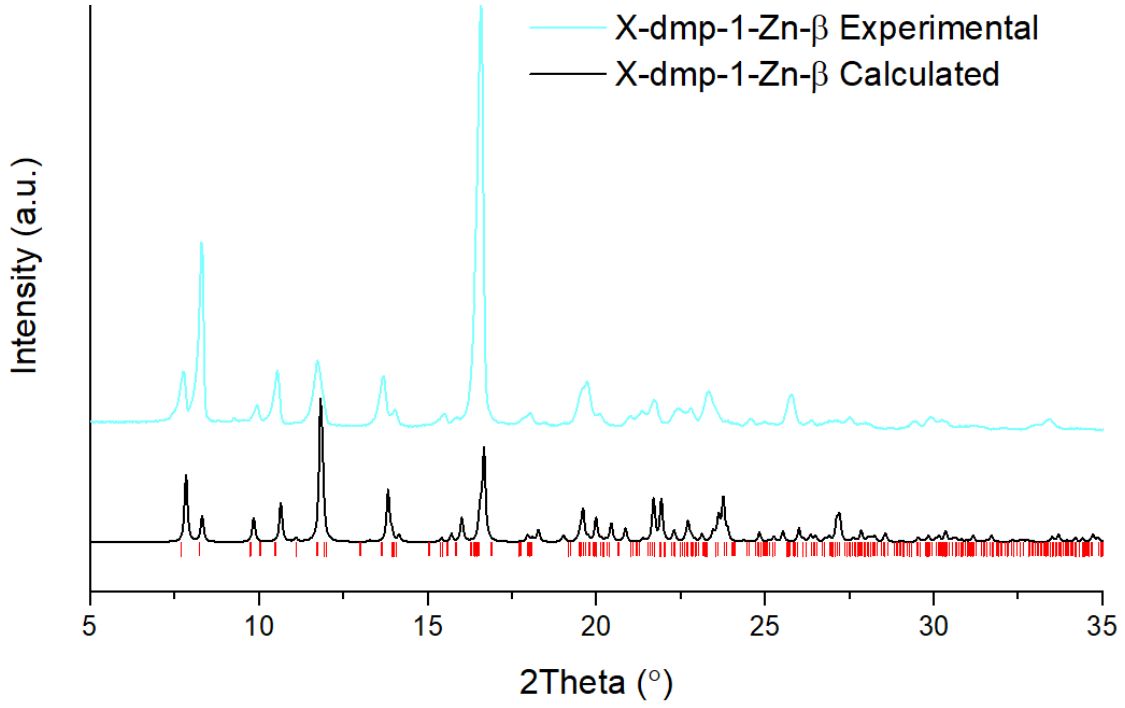

Fig. S8. PXRD patterns of **X-dmp-1-Zn-β** calculated from the crystal structure (black), and the experimental pattern (light cyan) of **X-dmp-1-Zn-β**, showing that the SCXRD structure is representative of the bulk material.

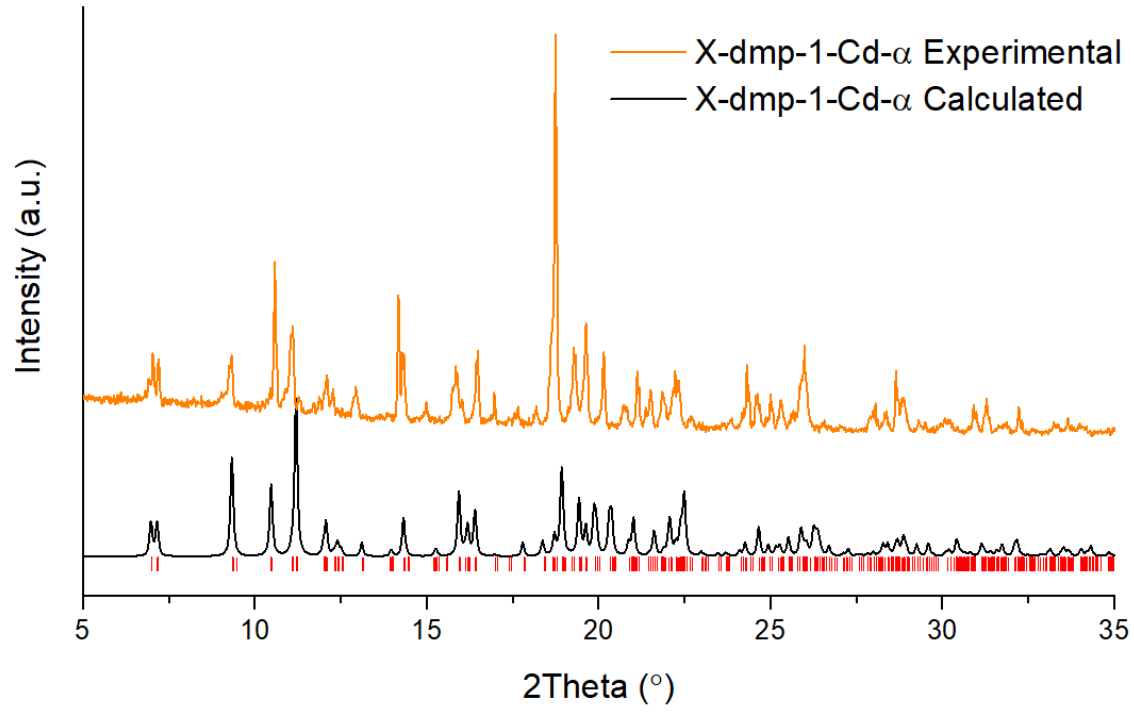

Fig. S9. PXRD patterns of **X-dmp-1-Cd-α** calculated from the crystal structure (black), and the experimental pattern (orange) of **X-dmp-1-Cd-α**, showing that the SCXRD structure is representative of the bulk material.

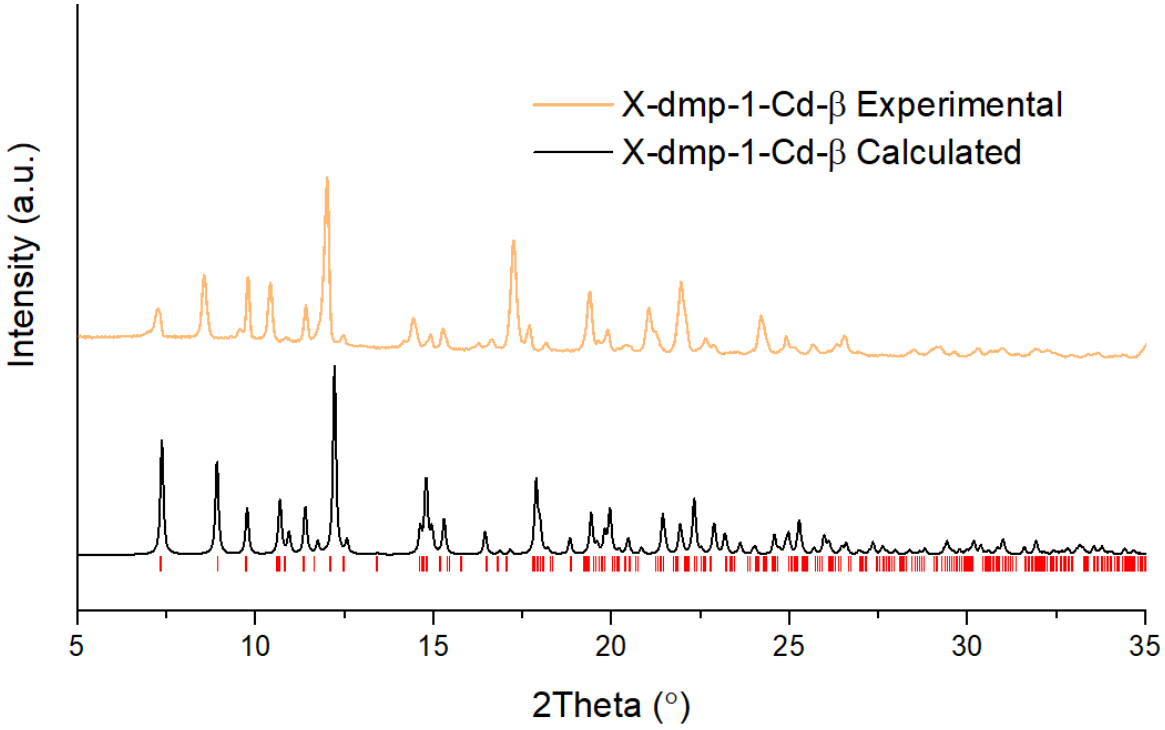

Fig. S10. PXRD patterns of **X-dmp-1-Cd-β** calculated from the crystal structure (black), and the experimental pattern (light orange) of **X-dmp-1-Cd-β**, showing that the SCXRD structure is representative of the bulk material.

5. Thermogravimetric Analysis (TGA)

Thermogravimetric analyses (TGA) were performed under N_2 using a TA Instruments Q50 system. A sample was loaded into an aluminium sample pan and heated at 10°C min^{-1} from room temperature to 500 °C.

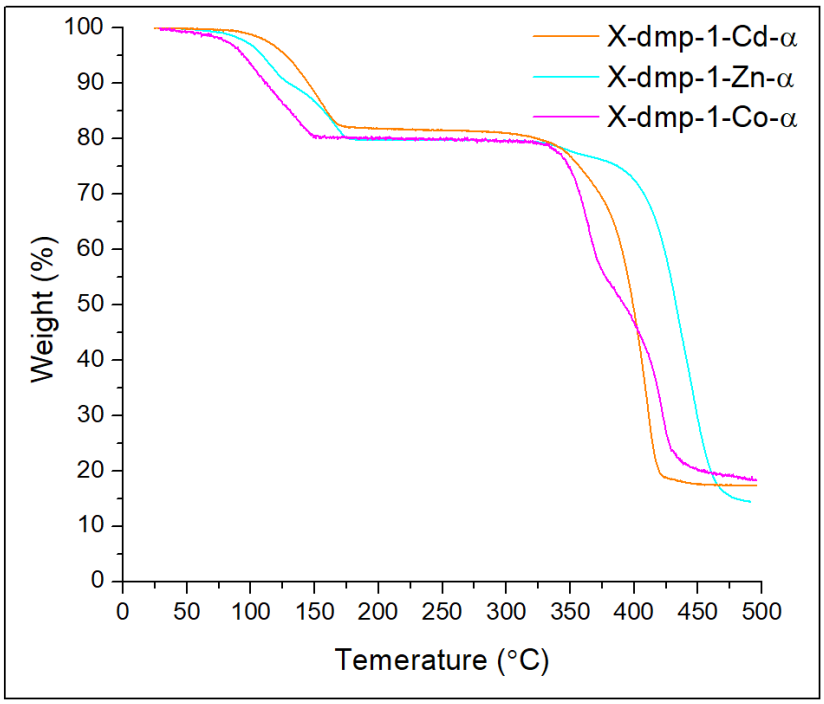

Fig. S11. Overlaid thermogravimetric traces for **X-dmp-1-Co-α** (pink), **X-dmp-1-Zn-α** (blue) and **X-dmp-1-Cd-α** (orange) showing a 19.64%, 20.27% and 18.24% mass loss between 25-200 °C (corresponding to two DMF guest molecules per ASU). Each material is then stable until decomposition begins at 325 °C, 378 °C and 360°C respectively.

6. Gas Sorption Measurements

6.1 Isotherm Measurements

Prior to performing gas sorption experiments, a freshly prepared sample of each of the three **X-dmp-1-M-α** forms was placed in a quartz tube and degassed under secondary vacuum using a Micromeritics Smart VacPrep system at 70 °C for 24 hours to remove any remaining solvent molecules and yield three bulk samples of **X-dmp-1-M-β**. Isotherms were measured using a Micromeritics 3 Flex sorption analyser. Gases were used as obtained from BOC Gases Ltd. (Ireland), with the following certified purities: research-grade He (99.999%), CO_2 (99.995%), CH_4 (99.995%), and N_2 (99.998%). Bath temperatures of 77 K and 195 K were maintained using liquid nitrogen and a dry ice-acetone slurry respectively. A Julabo ME v.2 temperature controller was used to maintain bath temperatures in 273 K and 298 K experiments. Samples were activated between successive experiments for a minimum of 5 hours at 70 °C.

High pressure CO_2 and CH_4 sorption experiments were performed using a Hiden Isochema XEMIS microbalance. Activated samples of **X-dmp-1-M-β** were further outgassed under secondary vacuum for 3 hours *in situ* before isotherms were run. Excess adsorption and

desorption profiles were obtained after applying a buoyancy correction using the crystallographically determined density of the three activated forms of **X-dmp-1-M-β**. Temperatures were maintained at 273 K and 294 K using a Grant LT Ecocool 150 temperature controller.

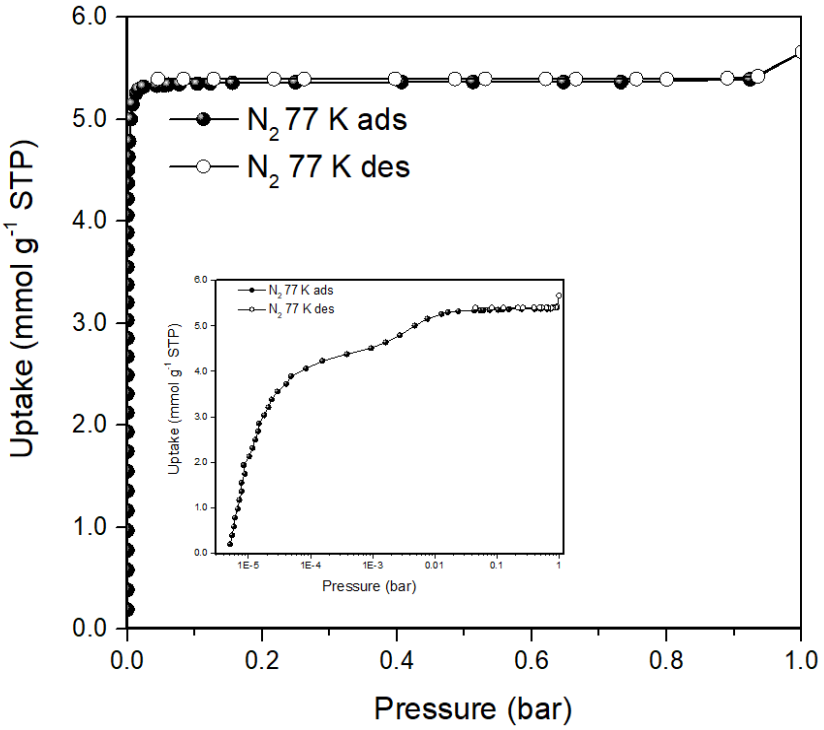

Fig. S12. N_2 gas sorption isotherm of **X-dmp-1-Co-β** at 77 K with insert showing log scale.

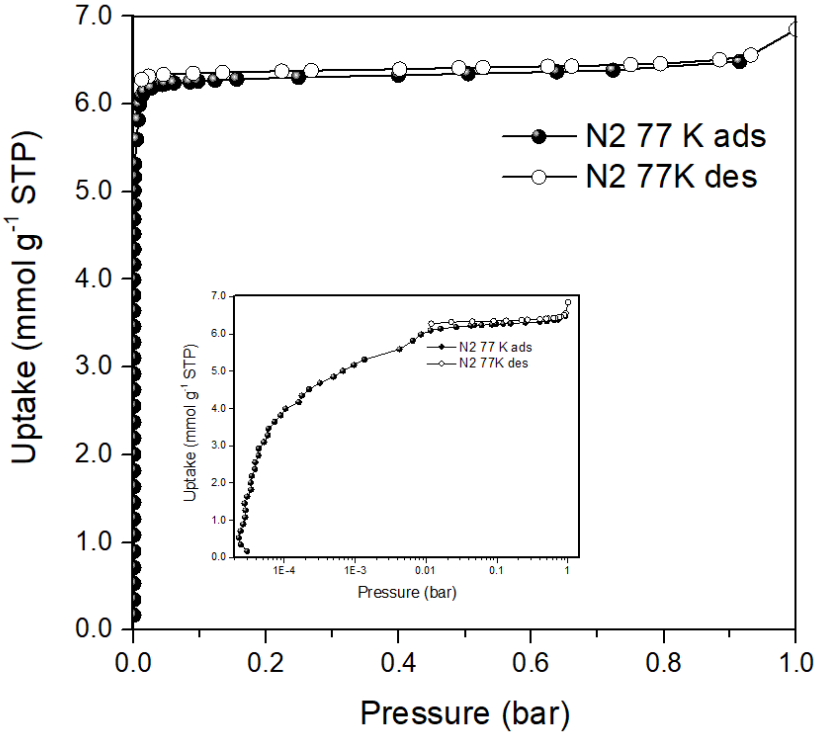

Fig. S13. N_2 gas sorption isotherm of **X-dmp-1-Zn-β** at 77 K with insert showing log scale .

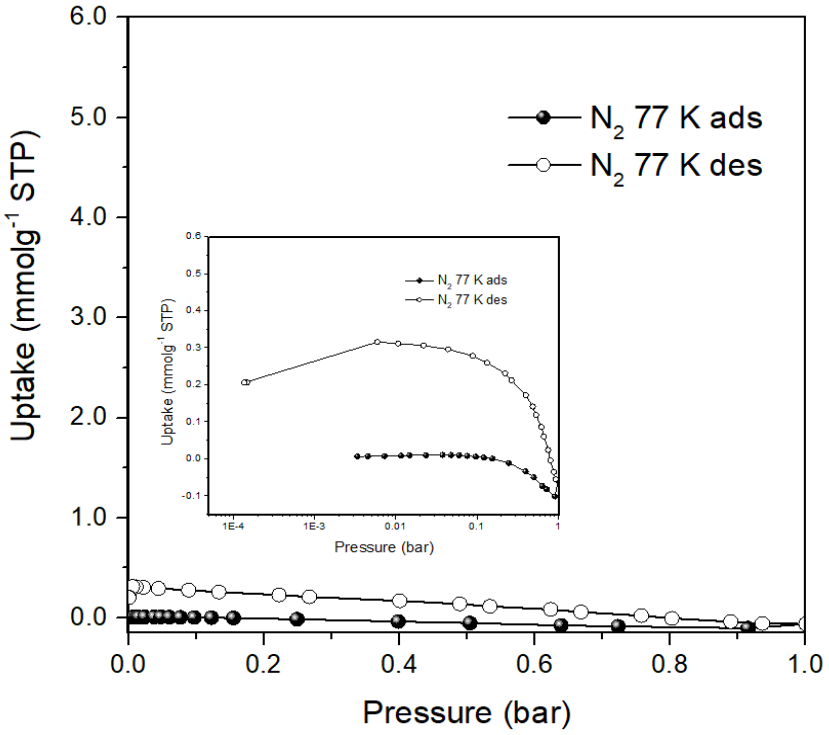

Fig. S14. N_2 gas sorption isotherm of **X-dmp-1-Cd-β** at 77 K with insert showing log scale .

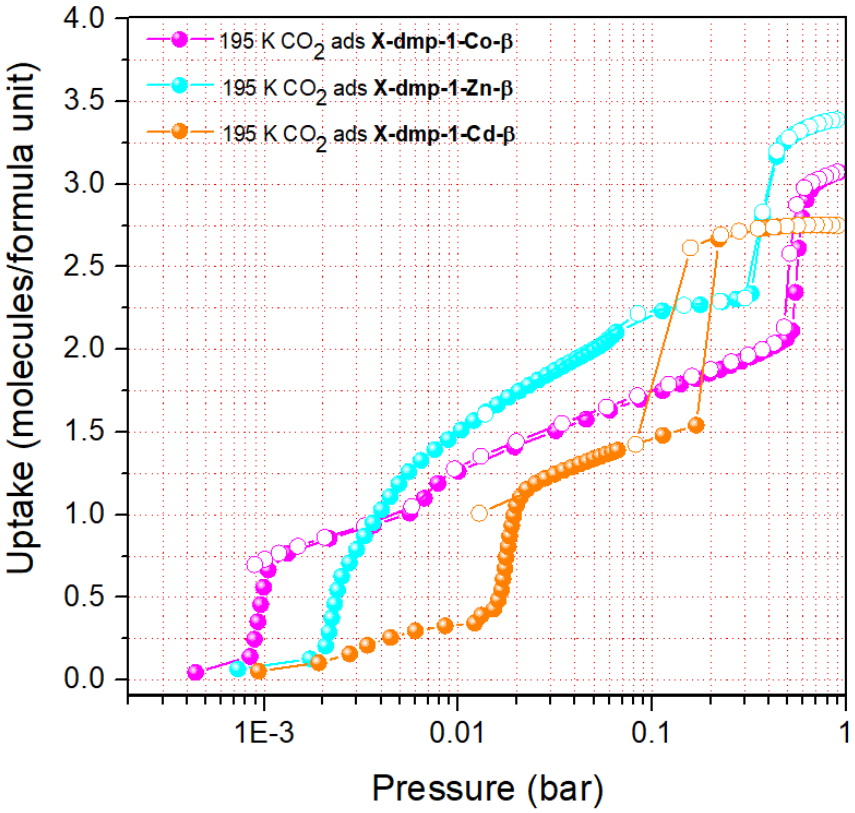

Fig. S15. Overlay of CO_2 gas sorption isotherms for all three forms of **X-dmp-1-M-β** at 195 K showing uptake as molecules per formula unit.

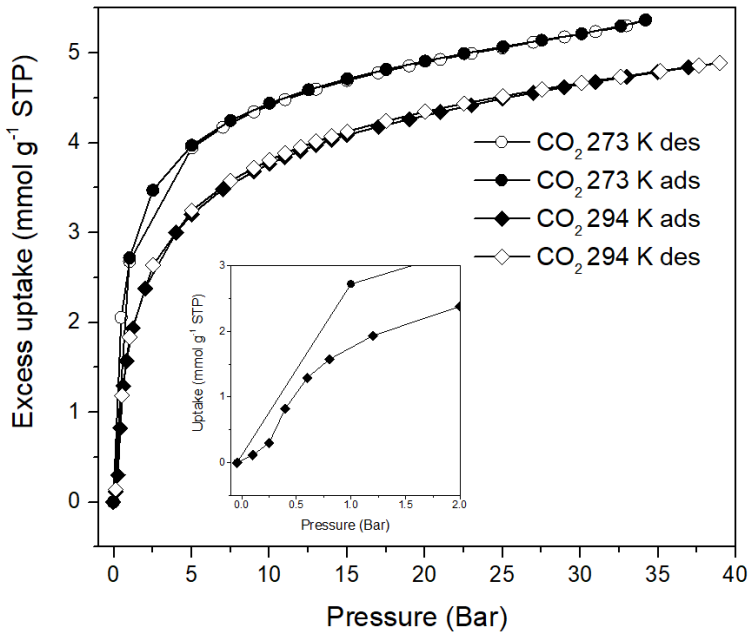

Fig. S16. High pressure CO_2 sorption isotherms of **X-dmp-1-Co-β** at 273 K (spheres) and 294 K (diamonds). Low pressure insert shows the transition of **X-dmp-1-Co-β** to **X-dmp-1-Co-γ1** at 294 K. Threshold uptake for final phase transition (**X-dmp-1-Co-γ3**) is not accessible at 273 K, even at P/P_0 = 1 (P = 34200 mbar).

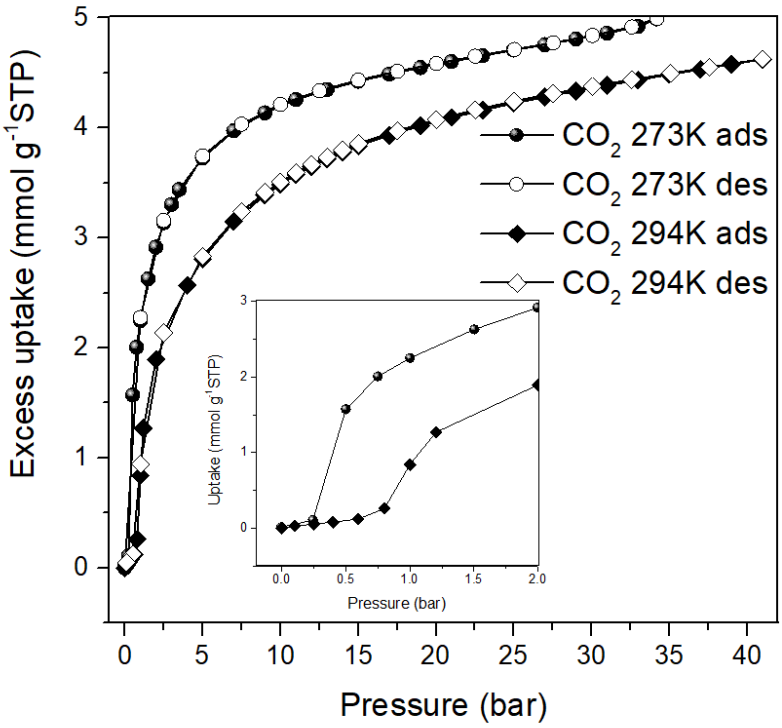

Fig. S17. High pressure CO_2 sorption isotherms of **X-dmp-1-Zn-β** at 273 K (spheres) and 294 K (diamonds). Low pressure insert shows the transition of **X-dmp-1-Zn-β** to **X-dmp-1-Zn-γ2** at 294 K. Threshold uptake for final phase transition (**X-dmp-1-Zn-γ3**) is not accessible at 273 K, even at P/P_0 = 1 (P = 34200 mbar).

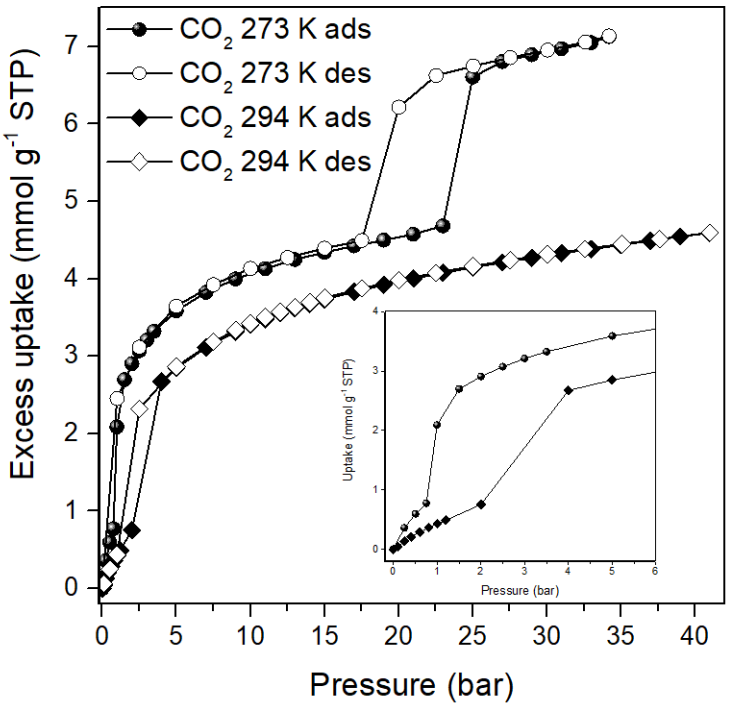

Fig. S18. High pressure CO_2 sorption isotherms of **X-dmp-1-Cd-β** at 273 K (spheres) and 294 K (diamonds). Low pressure insert shows the transition of **X-dmp-1-Cd-β** to **X-dmp-1-Cd-γ2** at 294 K. Threshold uptake for final phase transition (**X-dmp-1-Cd-γ3**) is observed at 23 bar at 273 K.

6.2 BET Surface Area

BET surface areas corresponding to 516.6 m²/g and 617.07 were determined from the 77 K N_2 sorption isotherms for **X-dmp-1-Co-β** and **X-dmp-1-Zn-β** (Fig. S14).[10] In the absence of appreciable N_2 uptake by **X-dmp-1-Cd-β**, the BET equation could not be applied.

Table S2. BET fit summary of the 77 K N_2 isotherm on **X-dmp-1-Co-β**.

BET surface area	516.61 ± 1.140 m²/g
Slope	0.00842 ± 0.00002 g/cm³ STP
Y-intercept	0.000002 ± 0.000000 g/cm³ STP
C	3,651.572
Q_m	118.69 cm³/g STP
Correlation coefficient	>0.9999

Table S3. BET fit summary of the 77 K N_2 isotherm on **X-dmp-1-Zn-β**.

BET surface area	617.07 ± 3.42 m^2/g
Slope	0.00705 ± 0.00004 g/cm^3 STP
Y-intercept	0.000004 ± 0.000000 g/cm^3 STP
C	1719.736
Q_m	141.77 cm^3/g STP
Correlation coefficient	>0.9999

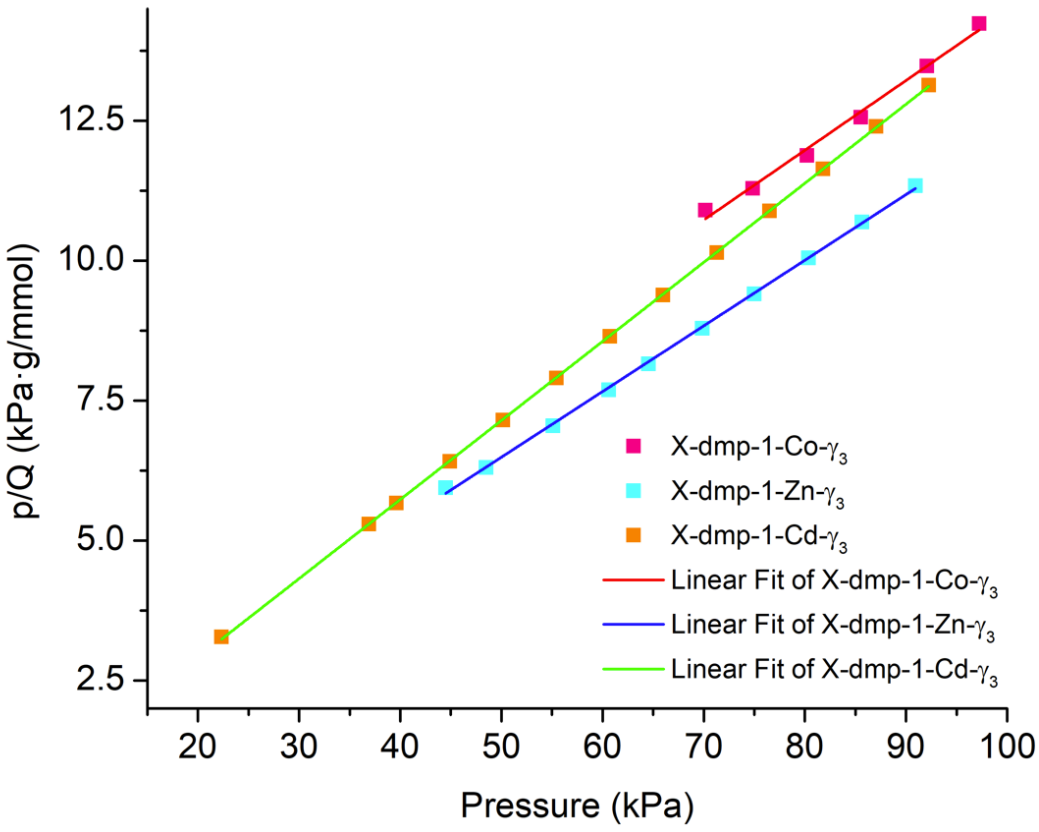

Fig. S19.Langmuir model fitting of 195 K CO_2 of **X-dmp-1-M**.

Table S4. BET fit summary of the 195 K CO_2 isotherms on **X-dmp-1-M**.

	X-dmp-1-Co-γ3	**X-dmp-1-Zn-γ3**	**X-dmp-1-Cd-γ3**
Langmuir surface area (m^2/g)	821.1779 ± 35.9386	872.7161 ± 7.3035	724.6935 ± 1.3339
Slope (g/mmol)	0.12467 ± 0.00546	0.11731 ± 0.00098	0.14127 ± 0.00026
Y-intercept (kPa·g/mmol)	1.996 ± 0.458	0.620 ± 0.068	0.078 ± 0.017
b constant (kPa^{-1})	0.06246	0.18912	1.80745
Q_m (mmol/g)	8.02113	8.52454	7.07868
Correlation coefficient	0.996191	0.999720	0.999981
Molecular cross-sectional area (nm^2)	0.1700	0.1700	0.1700

7. *In situ* Powder Xray diffraction

In-situ simultaneous PXRD measurements were conducted on a Rigaku Smartlab with CuKα radiation (Rigaku, Japan) which is synchronised to a BELSORP-18PLUS volumetric adsorption instrument (MicrotracBEL Japan, Corp.). A Helium-based cryosystem was connected to the sorption equipment to control the temperature range. The as-synthesised samples were soaked in MeOH for three days and then activated at 70 °C under vacuum overnight using a copper plate holder. The activated sample of ~70 mg was transferred to the sorption instrument and treated again under vacuum at 80 °C for 2 h.

The second activation was performed to remove any adsorbed moisture during transfer. This is an essential step as the sample adsorbs water from the atmosphere. Three CO_2 sorption experiments were carried out up to 100 kPa at 195 K. *In-situ* PXRD patterns were measured simultaneously at each equilibrium point of the adsorption and desorption isotherm.

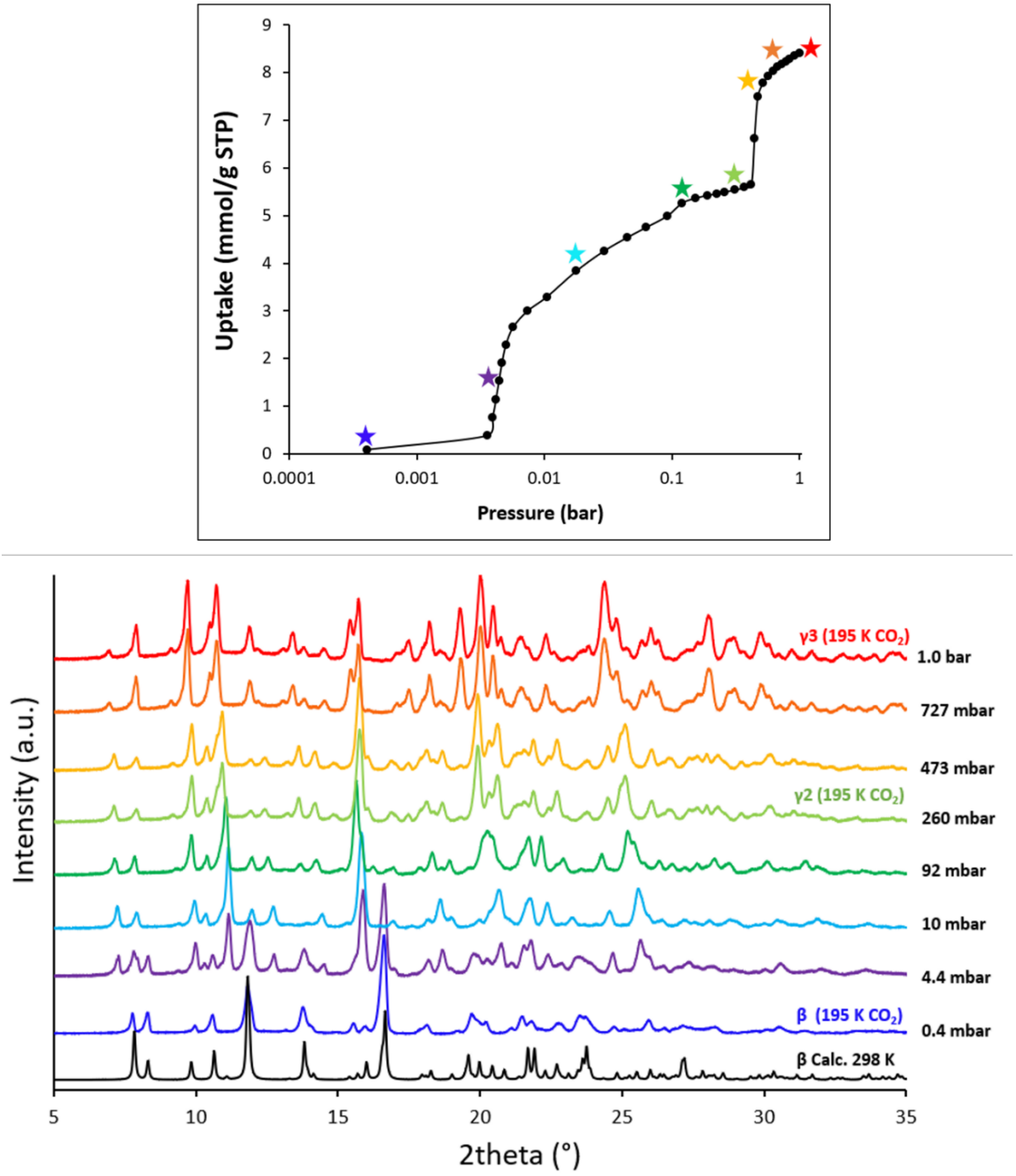

Fig. S20. (Top) **X-dmp-1-Zn-β** undergoes two transitions from closed to progressively more gas loaded forms **X-dmp-1-Zn-γ2** (cyan star) and **X-dmp-1-Zn-γ3** (red star)**.** (Bottom) Selected *in situ* variable pressure PXRD patterns of **X-dmp-1-Zn-β** at different CO_2 adsorption loadings at 195 K.

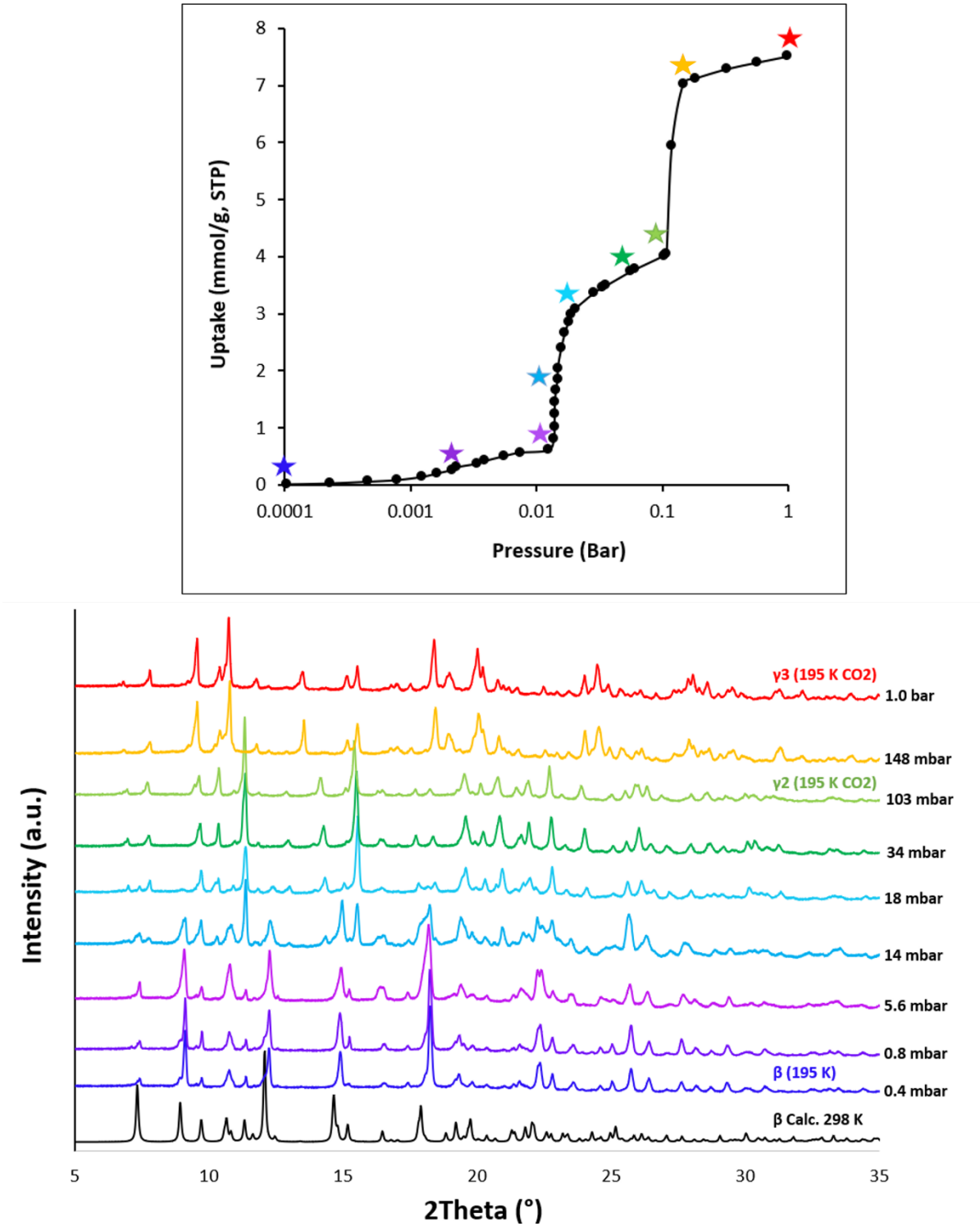

Fig. S21. Selected *in situ* variable pressure PXRD patterns of **X-dmp-1-Cd-β** at different CO_2 adsorption loadings at 195 K. **X-dmp-1-Cd-β** undergoes two transitions from closed to progressively more gas loaded forms **X-dmp-1-Cd-γ2** and **X-dmp-1-Cd-γ3.**

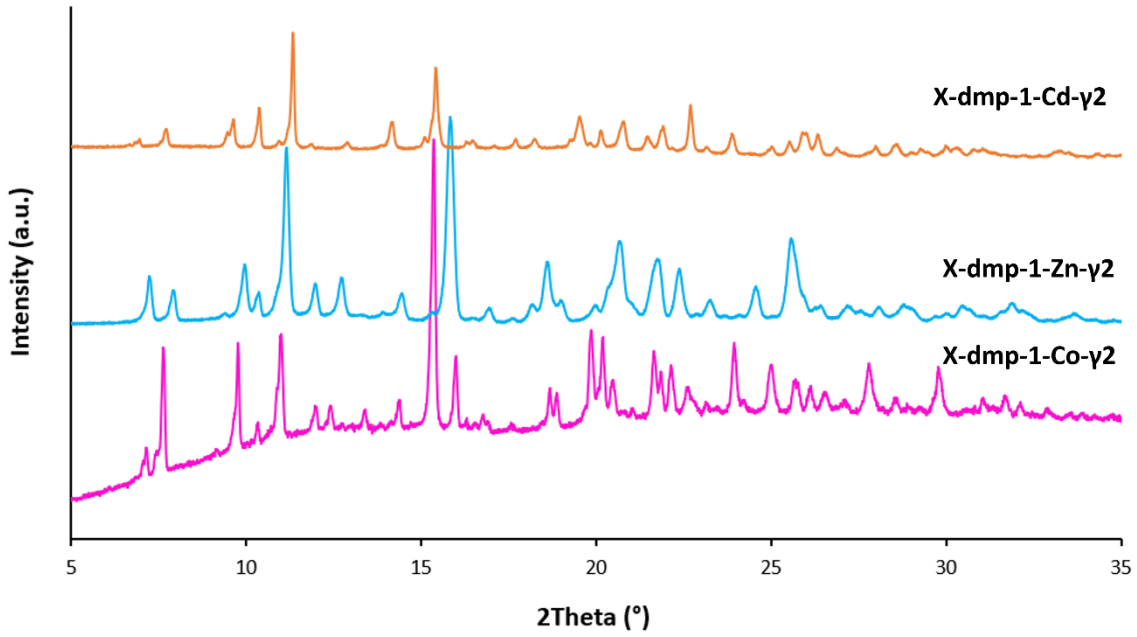

Fig. S22. Overlay of *in situ* variable pressure PXRD patterns of **X-dmp-1-Co-γ2** (pink) with **X-dmp-1-Zn-γ2** (blue) and **X-dmp-1-Cd-γ2** (orange)

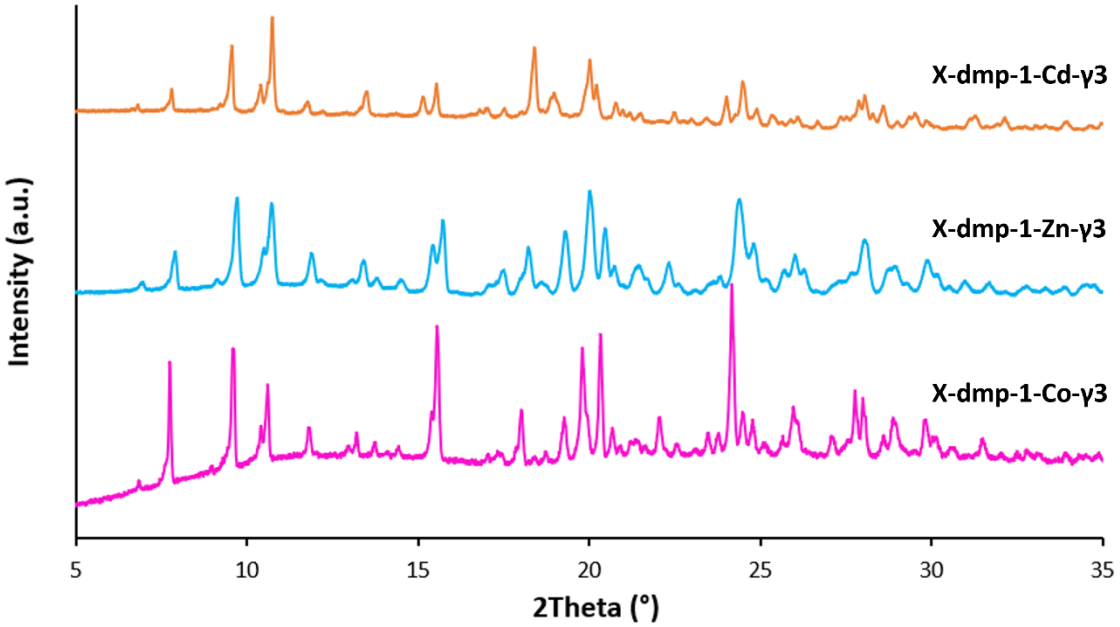

Fig. S23. Overlay of *in situ* variable pressure PXRD patterns of **X-dmp-1-Co-γ3** (pink) with **X-dmp-1-Zn-γ3** (blue) and **X-dmp-1-Cd-γ3** (orange).

8. Water Sorption

Water vapor sorption experiments were performed by using a dynamic vapor sorption (DVS) intrinsic analyzer (from Surface Measurement Systems, London, UK). The DVS Intrinsic is designed to accurately measure sample's mass change as the instrument sorbs precisely controlled concentrations of water vapor using air as a carrier gas. Each sample (~10 mg) was loaded into a stainless-steel pan and suspended from an ultra-sensitive recording microbalance (with a resolution of 0.1 mg) with the help of a hang-down wire. Before each experiment started, once the sample was loaded from said hang-down wire, it was allowed to reach temperature and humidity equilibria within its chamber for a short period of time. The sample was exposed to an air flow with known % RH (from 0 % RH to 90 % RH) with increasing/decreasing steps of 10 % RH in the adsorption/desorption branches, respectively. The flow rate used in the experiments was 200 sccm, and the temperatures employed were 298 K. Equilibria determination of the sample mass at each RH stage was performed by measuring the change rate percentage of mass over time (dm/dt). Not until said (dm/dt) reached a value of 0.002 % min^{-1}, the equilibria was considered to be achieved (with an accuracy of ± 1.0 % RH), and the device was allowed to measure the next point of RH. Accordingly, the sample mass readings obtained from the microbalance within said equilibria revealed the vapour adsorption/desorption behaviour of the sample. Consequently, isotherm analysis profiles of water vapor sorption and desorption were recorded.

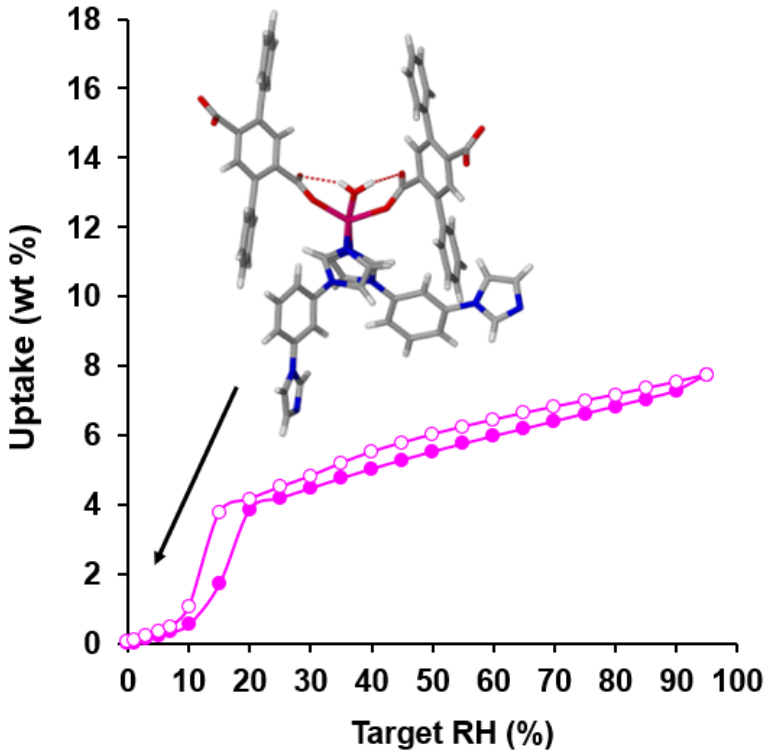

Fig. S24. S-shaped water vapour adsorption isotherms for **X-dmp-1-Co** with immediate irreversible conversion to water-inserted phase performed at 27 °C using an Adventure Dynamic Vapour Sorption (DVS).

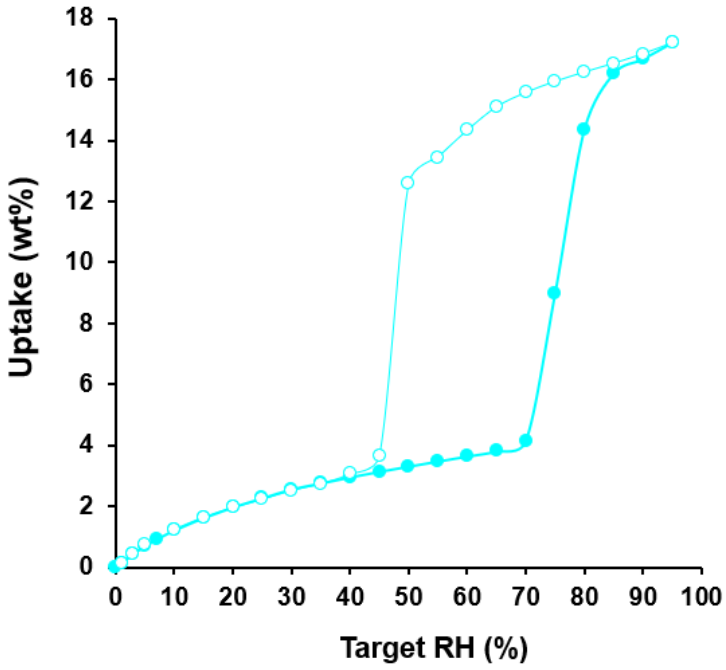

Fig. S25. S-shaped water vapour adsorption isotherms for **X-dmp-1-Zn** performed at 27 °C using an Adventure Dynamic Vapour Sorption (DVS).

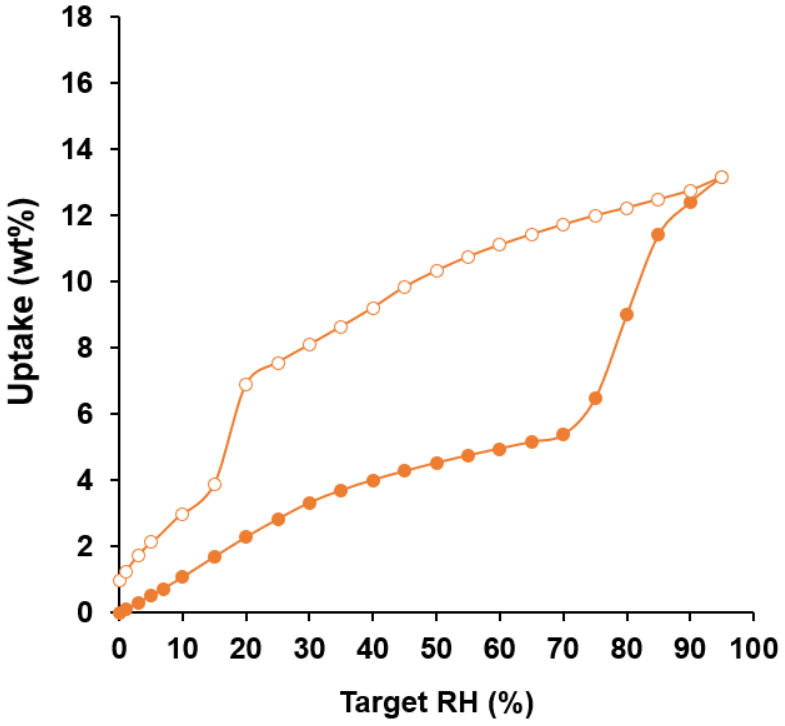

Fig. S26. S-shaped water vapour adsorption isotherms for **X-dmp-1-Cd** performed at 27 °C using an Adventure Dynamic Vapour Sorption (DVS)

9. Methane-induced Switching Materials

Table S5. CH_4 sorption parameters for representative switching coordination networks.

Compound	CH_4 Uptake (g/g)	CH_4 Uptake (cc/cc)	Temp. (K)	Loading Pressure (bar)	CH_4 Working Capacity (g/g)	CH_4 Working Capacity (cc/cc)	Gate Opening Pressure (bar)	Ref.
$Cu_2(bdc)_2(bpy)$	0.056[a]	62.5[a]	298	35	0.052[a]	58.2[a]	9	13
$Cu(dhbc)_2(bpy)$	0.055[a]	98[a]	298	65	0.054[a]	93.7[a]	8	14
$Cu(bpy)_2(BF_4)$	0.061[a]	NR	303	63	0.059[b]	NR	38	15
MIL-53(Fe)	0.031[a]	NR	303	30	0.030[a]	NR	10	16
MIL-53(Al)-NH_2	0.085	121	298	65	0.081	115	24	17
MIL-53(Al)-OH	0.155	217	298	65	0.118	164	15	18
MIL-53(Al)-$(OH)_2$	0.066	96	298	65	0.051	71	53	19
Co(bdp)	0.187	203	298	65	0.183	197	16	20
Fe(bdp)	0.206	196	298	65	0.2	190	24	20
Co(F-bdp)	0.123[b]	125[b]	298	40	0.109[b]	111[b]	5.7	21
Co(p-F2-bdp)	0.113[b]	124[b]	298	40	0.11[b]	120.5[b]	10	21
Co(o-F2-bdp)	0.115[b]	119[b]	298	40	0.112[b]	115.6[b]	11	21
Co(D4-bdp)	0.128[b]	128[b]	298	40	0.126[b]	126[b]	18	21
X-dia-1-Ni	0.158	189	298	65	0.125	149	20	22
ZIF-7	NR	95	303	60	NR	90	10	23
ZIF-9	NR	96	303	60	NR	90	15	23
X-dmp-1-Co	[b]	[b]	**298**	**35**	[b]	[b]		
X-dmp-1-Zn	[b]	[b]	**298**	**35**	[b]	[b]		
X-dmp-1-Cd	[b]	[b]	**298**	**35**	[b]	[b]		
a = unspecified uptake calculation								
b = excess uptake								

10. References

1 Merlet, S.; Birau, M.; Wang, Z.Y., *Org. Lett.,* 2002, **4**, 2157-2159.

2 SMART Data Collection Software, Version 5.629, Bruker AXS Inc., Madison, WI, 2003.

3 SAINT Data Reduction Software, Version 6.45, Bruker AXS Inc., Madison, WI, 2003.

4 SADABS, Bruker AXS Inc., Madison, WI, 2014.

5 Sheldrick, G. M. *Acta Crystallogr., Sect. C*, 2015, **71**, 3-8.

6 Barbour, L. J., *J. Supramol. Chem*., 2001, **1**, 189-191.

7 a) Connolly, M. L., *Science*, 1983, **221**, 709-713; b) Connolly, M. L., *J. Mol. Graphics*, 1993, **11**, 139-141.

8 Degen, T.; Sadki, M.; Bron, E.; König, U.; Nénert, G., *Powder Diffr*., 2014, **29**, S13-S18.

9 Macrae, C. F.; Bruno, I. J.; Chisholm, J. A.; Edgington, P. R.; McCabe, P.; Pidcock, E.; Rodriguez-Monge, L.; Taylor, R.; van de Streek, J.; Wood, P. A., *Appl. Crystallogr*., 2008, **41**, 466-470.

10 Thommes, M.; Kaneko, K.; Neimark, A.; Olivier, V.; Rodriguez-Reinoso, J. P.; Rouquerol, F.; Sing, J., *Pure Appl. Chem*., 2015, **87**, 1051-1069.

11 a) Altomare, A.; Cuocci, C.; Giacovazzo, C.; Moliterni, A.; Rizzi, R.; Corriero N. and Falcicchio, A., *J. Appl. Cryst*., 2013, **46**, 1231-1235; b) Altomare, A.; Camalli, M.; Cuocci, C.; Giacovazzo, C.; Moliterni, A.; Rizzi, R., *J. Appl. Cryst*., 2009, **42**, 1197-1202.

12 Li, L.; Krishna, R.; Wang, Y.; Yang J.; Wanga, X.; Li, J., *J. Mater. Chem. A*, 2016, **4**, 751-755.

13. Seki, K., *Phys. Chem. Chem. Phys*., 2002, **4**, 1968–1971.

14. Kitaura, R.; Seki, K.; Akiyama, G.; Kitagawa, S., *Angew. Chem. Int. Ed*., 2003, **42**, 428-431.

15. Noguchi, H.; Kondoh, A.; Hattori, Y.; Kanoh, H.; Kajiro, H.; Kaneko, K., *J. Phys. Chem. B*, 2005, **109**, 13851-13853.

16. Llewellyn, P. L.; Horcajada, P.; Maurin, G.; Devic, T.; Rosenbach, N.; Bourrelly, S.; Serre, C.; Vincent, D.; Loera-Serna, S.; Filinchuk, Y.; Férey, G., *J. Am. Chem. Soc*., 2009, **131**, 13002-13008.

17. Bolinois, L.; Kundu, T.; Wang, X.; Wang, Y.; Hu, Z.; Koh K.; Zhao, D., *Chem. Commun*., 2017, **53**, 8118-8121.

18. Kundu, T.; Shah, B. B.; Bolinois, L.; Zhao, D., *Chem. Mater*., 2019, **31**, 2842−2847.

19. Liang, J.; Li, X.; Xi, R.; Shan, G.; Li, P.-Z.; Liu, J.; Zhao, Y.; Zou, R.; *ACS Materials Lett*., 2020, **2**, 220-226.

20. Mason, J. A.; Oktawiec, J.; Taylor, M. K.; Hudson, M. R.; Rodriguez, J.; Bachman, J. E.; Gonzalez, M. I.; Cervellino, A.; Guagliardi, A.; Brown, C. M.; Llewellyn, P.L.; Masciocchi, N.; Long, J. R., *Nature*, 2015, **527**, 357-361.

21. Taylor, M. K.; Runčevski, T.; Oktawiec, J.; Gonzalez, M. I.; Siegelman, R. L.; Mason, J. A.; Ye, J.; Brown, C. M.; Long, J. R., *J. Am. Chem. Soc*., 2016, **138**, 15019−15026.

22. Yang, Q.-Y.; Lama, P.; Sen, S.; Lusi, M.; Chen, K.-J.; Gao, W.-Y.; Shivanna, M.; Pham, T.; Hosono, N.; Kusake, S.; Perry IV, J. J.; Ma, S.; Space, B.; Barbour, L. J.; Kitagawa, S.; Zaworotko, M. J., *Angew. Chem. Int. Ed*., 2018, **57**, 5684-5689.

23. McGuirk, C. M.; Runčevski, T.; Oktawiec, J.; Turkiewicz, A.; Taylor, M. K. Long, J. R., *J. Am. Chem. Soc*., 2018, **140**, 15924−15933.

24. Kresse, G.; Furthmuller, J., *Comput. Mater. Sci.,* 1996, **6**, 15-50.

25. Kresse, G.; Furthmuller, J., *Phys. Rev. B*, 1996, **54**, 11169-11186.

26. Perdew, J. P.; Burke, K.; Ernzerhof, M., *Phys. Rev. Lett.*, 1997, **78**, 3865-3868.

27. Wellendorff, J.; Lundgaard, K. T.; Møgelhøj, A.; Petzold, V.; Landis, D. D.; Nørskov, J. K.; Bligaard, T.; Jacobsen K. W., *Phys. Rev. B*, 2012, **85**, 235149.

28. Blochl, P. E., *Phys. Rev. B*, 1994, **50**, 17953-17979.

29. Pack, J. D.; Monkhorst, H. J., *Phys. Rev. B*, 1977, **16**, 1748.

30. Monkhorst, H. J.; Pack, J. D., *Phys. Rev. B*, 1976, **13**, 5188.